JOURNAL OF CATALYSIS 139, 104–118 (1993)

Estimates of the Rate Coefficients for Chain Initiation, Propagation, and Termination during Fischer–Tropsch Synthesis over Ru/TiO_2

KAMALA R. KRISHNA AND ALEXIS T. BELL

Center for Advanced Materials, Lawrence Berkeley Laboratory and Department of Chemical Engineering, University of California, Berkeley, California 94720

Received January 29, 1992; revised July 21, 1992

Transient response isotopic tracer experiments have been used to study chain growth during Fischer–Tropsch synthesis over an Ru/TiO_2 catalyst. This involves observation of the incorporation of ^{13}C into reaction products after an abrupt switch from $^{12}CO/D_2$ to $^{13}CO/D_2$ in the feed. Values for the rate coefficients for initiation, propagation, and termination are determined by fitting theoretically generated model curves to the observed transient responses. The rate coefficient for chain initiation is independent of temperature and D_2/CO ratio. The rate coefficients for propagation and termination increase with temperature. The rate constant for propagation is not affected by the D_2/CO ratio. The rate coefficient for termination increases linearly with increasing D_2/CO ratio. The activation energy for chain propagation is 8 kcal/mol, whereas the activation energy for chain termination is 20 kcal/mol. The relative values of these two activation energies explains the observed decrease in chain growth probability, α, with increasing temperature. Coverages by reaction intermediates are also estimated. The dominant species are monomeric building units which occupy 0.3–0.6 ML. Alkyl species that are the direct hydrocarbon product precursors occupy < 0.2 ML and adsorbed CO covers 0.7 ML.

INTRODUCTION

Fischer–Tropsch synthesis (FTS) produces a spectrum of products consisting primarily of linear olefins and alkanes (*1*). The carbon number distribution of the products containing four or more carbon atoms is often well described by an Anderson–Schulz–Flory (ASF) distribution, which assumes that products containing n carbon atoms are produced by a stepwise polymerization of C_1 species (*2*). If the probability of chain growth, α, defined as the ratio of the rate of chain propagation to the sum of the rates of chain propagation and termination, is taken to be independent of n, then $[N_{Cn+1}]/[N_{Cn}] = \alpha$, where N_{Cn} and N_{Cn-1} are the turnover frequencies for products containing n and $n + 1$ carbon atoms, respectively. Steady-state investigations of FTS have shown that α is a complex function of both temperature and the partial pressures of H_2 and CO (*2–5*).

Mechanistic studies of hydrocarbon production by FTS over Fe, Co, and Ru suggest that the mechanism of FTS might be described by the following reaction sequence (*6*):

1. $CO_g \rightleftarrows CO_s$
2. $H_{2,g} \rightleftarrows 2H_s$
3. $CO_s \rightarrow C_s + O_s$
4. $O_s + H_s \rightarrow OH_s$
5. $H_s + H_s \rightarrow H_2O_s$
6. $C_s + H_s \rightleftarrows CH_s$
7. $CH_s + H_s \rightleftarrows CH_{2,s}$
8. $CH_{2,s} + H_s \rightleftarrows CH_{3,s}$
9. $CH_{3,s} + H_s \rightarrow CH_{4,g}$
10. $CH_{3,s} + CH_{2,s} \rightarrow CH_3CH_{2,s}$
11. $CH_3CH_{2,s} + H_s \rightarrow CH_3CH_{3,g}$
12. $CH_3CH_{2,s} \rightarrow CH_2CH_{2,g} + H_s$
13. $CH_3CH_{2,s} + CH_{2,s} \rightarrow CH_3CH_2CH_{2,s}$

. . .

14. $C_nH_{2n+1,s} + CH_{2,s} \rightarrow C_{n+1}H_{2(n+1)+1,s}$
15. $C_nH_{2n+1,s} + H_s \rightarrow C_nH_{2n+2,g}$
16. $C_nH_{2n+1,s} \rightarrow C_nH_{2n,g} + H_s$.

0021-9517/93 $5.00

Adsorbed CO covers most of the catalyst surface and is in equilibrium with gas-phase CO (*6–8*). Likewise, dissociatively adsorbed H_2 is found to be in equilibrium with gas-phase H_2 (*8*). Some of the adsorbed CO dissociates irreversibly (*7, 9*) to form C_s and O_s. The atomic oxygen produced in this manner reacts rapidly with H_s to form water, whereas the atomic carbon reacts with hydrogen to form CH_x ($x = 1–3$) species (*9, 10*). The $CH_{3,s}$ species can react with additional hydrogen to form CH_4 or react with a $CH_{2,s}$ species, thereby initiating the process of chain growth. Chain propagation is sustained by $CH_{2,s}$ addition to adsorbed alkyl species. Chain termination can occur by hydrogen addition to a surface alkyl species to give a paraffin or by hydrogen abstraction to give an olefin.

A number of investigators have used isotopic-tracer techniques to identify the species involved in the chain growth process and to estimate the rate coefficients for chain propagation and termination (*7, 11–20*). In studies conducted with a Ru/SiO_2 catalyst, Kobori *et al.* (*11*) concluded that hydrocarbons are formed by the polymerization of CH_x intermediates and that CO insertion plays no part in the chain growth process leading to hydrocarbons. Work by Biloen *et al.* (*12*) on unsupported Co, Ni/SiO_2, and $Ru/\gamma\text{-}Al_2O_3$ has shown that carbidic intermediates are involved in the reaction and that methane and higher hydrocarbons have a common precursor. Stockwell and Bennett (*17*) were unable to conclude whether chain growth occurred via a CO insertion or a CH_x insertion mechanism. Studies on an Fe/Al_2O_3 catalyst by Stockwell *et al.* (*18*) implicated a CH species as responsible for chain growth. The authors concluded that once chain growth is initiated, the production of methane and C_{2+} hydrocarbon becomes rapid and the coverage by growing chains becomes small.

Several attempts to determine the rate coefficients for chain propagation and termination have been reported. Zhang and Biloen (*14*) have looked at the successive incorporation of ^{13}C into C_{1-3} hydrocarbon products over Co and Ru catalysts. For Co, it was estimated that at 483 K, the value of the apparent rate constant for propagation decreased from 0.045 to 0.025 s^{-1} and the corresponding value of the apparent rate constant for chain termination increased from 0.02 to 0.04 s^{-1}, as the D_2/CO ratio increased from 1 to 6.55. For the same reaction conditions, the coverage by alkyl chains was estimated to be between 0.19 and 0.25 ML, whereas the coverage by monomeric species was much smaller. For Ru, the apparent rate coefficient for chain propagation was estimated to be ≥ 1 s^{-1}. Based on similar experiments, Mims and McCandlish (*15*) have estimated the apparent rate coefficient for chain propagation to be 2–4 s^{-1} for a promoted Fe catalyst at 510 K and an H_2/CO ratio of 1 (*15*), and 2 s^{-1} on Co at 475 K and an H_2/CO ratio of 2 (*16*). Over both Fe and Co, the coverage by the monomeric species exceeded the coverage by hydrocarbon chains. In a recent study using a Ru/TiO_2 catalyst, Yokomizo and Bell (*21*) observed that 80% of the carbidic species on the Ru surface served as a monomer building block and 20% acted as the precursor to methane. The rate coefficient for chain termination was estimated to be 0.044 s^{-1} at $T = 463$ K, $p_{CO} = 50$ Torr and $D_2/CO = 3$. The total coverage by C_1 species was reported to be 0.25 ML, and the coverage by C_{2+} species leading to hydrocarbon product was estimated at 0.1 ML.

The objective of the present investigation is to estimate the rate coefficients for chain initiation, propagation, and termination, and to study their dependence on temperature and D_2/CO ratio. A further aim of this effort is to determine the surface coverages by the various reactive carbonaceous species present on the catalyst. A Ru/TiO_2 catalyst was used for these investigations because of the high specific activity of Ru for FTS and its characteristically high value of α (*22*). The absence of alcohols from the products of FTS over Ru was a further reason for choosing this metal. Titania was

used to support and disperse the ruthenium, since titania-supported Group VII metals are known to be more active than silica- or alumina-supported Group VIII metals (*23–26*).

EXPERIMENTAL

Catalyst Preparation and Characterization

A 3.3% Ru/TiO_2 catalyst was prepared by incipient wetness impregnation of Degussa P-25 titania with an aqueous solution of $RuCl_3 \cdot H_2O$ (Strem). Details of the preparation are given in Ref. (*27*). The dried catalyst was reduced at 503 K to minimize encapsulation of the Ru crystallites by titania. The metal content of the catalyst was determined by X-ray fluorescence. The chloride level after reduction was below the detection limit (0.02%). The dispersion of Ru was determined by H_2 chemisorption to be 15.5%, while the CO uptake on the freshly reduced catalyst was 1.3 ML. The BET surface area, determined from an N_2 isotherm at 77 K was 47.5 m^2/gm.

Apparatus

D_2, ^{12}CO, ^{13}CO, and He were supplied from a gas manifold to a low dead-volume quartz microreactor. UHP H_2 (Matheson Gas) or D_2 (Union Carbide) were further purified by passage through a Deoxo unit (Engelhard Industries) and water was removed by a molecular sieve 13X trap. UHP CO (99.999% pure, Matheson Gas) was passed through a glass bead trap maintained at 573 K to remove iron carbonyls, an Ascarite trap to remove CO_2, and a molecular sieve trap to remove water. UHP He was passed through a molecular sieve trap to remove water. ^{13}CO (Isotec Inc, 99% ^{13}C) was used as supplied.

Tylan mass-flow controllers were used to regulate the flow of all four gases. The ^{12}CO and ^{13}CO streams flow from the flow controllers into two separate low dead-volume, 2-position, 4-port valves. One stream from each of these valves flows through a bubblemeter to a vent line, while the other stream flows to a 4-way tee. He and D_2 are mixed and introduced into the third inlet of the 4-way tee, and the outlet from the tee goes to the microreactor. This flow scheme enables establishment of steady-state flow to the vent line in both CO streams and allows switching the reactor feed from one isotopically labeled form of CO to the other without significant flow perturbation. By simultaneous switching of the two 4-port valves, one avoids the elution of a small slug of the first isotope of CO held up in the valve and flow line.

Product Analysis

The steady-state distribution of reaction products was determined by gas chromatography and the temporal variation in the distribution of ^{12}C and ^{13}C in each product was determined by isotopic ratio gas chromatography–mass spectroscopy (*28–30*). Figure 1 shows a schematic of the analytical system. A 10-port GC sampling valve (Valco E410UWP) and a multiposition 16 sample-loop valve (Valco E6ST16T) were used to acquire and store samples. Both valves are housed in valve ovens and can be actuated electrically. Flow lines downstream of the reactor, the valve ovens, and lines to the GC inlet were all maintained at 393 K, to minimize product condensation.

Product analysis is initiated by injecting the contents of one of the sample loops into a Perkin–Elmer Sigma 3B chromatograph containing a fused silica capillary column (0.25 mm i.d. × 50 m) coated with a 1-μm film of SE-54. To achieve good product resolution, the column is maintained at 233 K for 4 min, then ramped at 20 K/min to 523 K, and finally held at 523 K for 10 min. This sequence results in a total sample analysis time of 28.5 min. C_{1-2} products elute at the initial temperature, C_{3-8} products elute during the temperature ramp, and C_{9-18} products elute at the final temperature. Products heavier than C_{14} hydrocarbons are not detected. The column effluent is split into two streams using a glass-lined capillary union (SGE); one line (0.11 mm i.d.) is sent to an

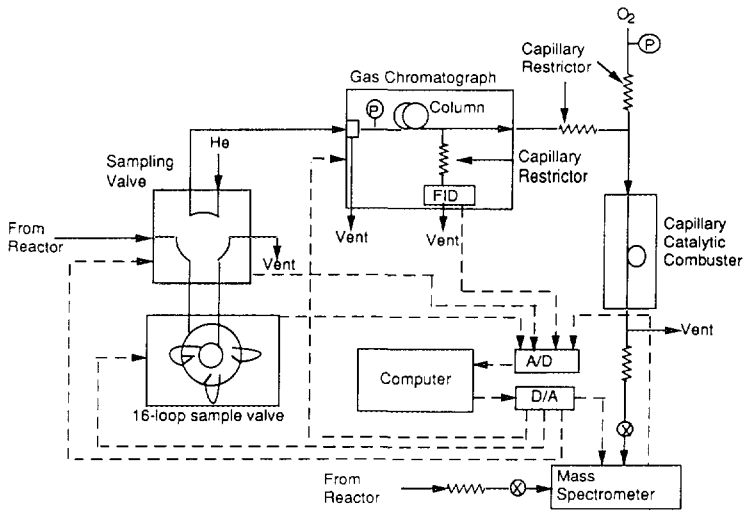

FIG. 1. Schematic of GC–MS analytical system.

FID detector for quantification, while the other transfer line (0.20 mm I.D.) is routed to a capillary combuster. This latter stream is mixed with O_2 and combusted to CO_2 in a 2-m-long capillary (0.2 mm i.d.) containing Pt wire (0.13 mm o.d.) maintained at 873 K. Details of the capillary combuster are given in Ref. (*30*).

The effluent from the combuster is leaked into a vacuum chamber containing the probe of a UTI 100C quadrupole mass spectrometer. The leak is accomplished by coupling the exit of the combuster directly to the inlet capillary restrictor of the mass spectrometer. The flow rate through the combuster is sufficient to preclude the back diffusion of air into the mass spectrometer. Complete combustion of all hydrocarbon products except methane was confirmed by the absence of peaks at masses corresponding to fragments derived from the hydrocarbons. The combustion of methane was found to be inhibited by the presence of a large amount of CO, which elutes at the same time as methane. The masses monitored by the mass spectrometer were amu 4 (He), amu 20 (D_2O and $^{12}CD_4$), amu 21 ($^{13}CD_4$), amu 44 ($^{12}CO_2$), and amu 45 ($^{13}CO_2$). The distribution of ^{12}C and ^{13}C in methane was determined from the relative intensities of the signals for amu 20 and amu 21. The presence of D_2O in the products, which also produces a signal at amu 20, did not interfere with the detection of $^{12}CD_4$, since CD_4 and D_2O elute at sufficiently different times. The distribution of ^{12}C and ^{13}C in C_{2+} hydrocarbons was obtained from the relative signal intensities at amu 44 and amu 45. The temporal resolution of these products recorded by the mass spectrometer was comparable to that recorded by the FID.

Operation of the sampling valves was controlled by an IBM PC/XT computer programmed to acquire samples at preset times. The computer was also used to record the output from the FID detector and the mass spectrometer at the rate of two data points a second.

Procedure

Experiments were carried out at temperatures between 453 K and 483 K. The ratio of D_2/CO was varied between 2 and 5, by holding the CO partial pressure at 0.1 atm and varying the D_2 partial pressure between 0.2 and 0.5 atm. The total flow rate to the reactor was 100 cm^3/min. CO conversions were maintained as low as possible and, in

most cases, were below 10%. For each set of conditions, the reaction was allowed to proceed in a mixture of ^{12}CO, D_2, and He for 20 min, to avoid the rapid initial loss in activity after start-up (*27*). Deactivation after the initial start-up proceeds with a first order decay time constant of 5 h. After each experiment, the catalyst was reduced in D_2/He at 523 K for 2 h to ensure that steady-state activity levels were maintained.

Isotopic-tracer, transient response experiments were initiated by switching the feed from a stream containing ^{12}CO to one containing an equivalent concentration of ^{13}CO, after steady-state conditions had first been achieved in ^{12}CO. In this fashion, the steady-state activity of the catalyst was not perturbed by the switch in isotopic label on the CO. To obtain good temporal resolution of the isotopic composition of the products, the following sampling sequence was used. A sample was taken 15 s after the switch in CO isotopic composition, followed by four samples taken at 10-s intervals, followed by a sample taken after an interval of 15 s, one taken after an interval of 20 s, one taken after an interval of 30 s, and two taken after intervals of 240 s. In this way, 11 samples are acquired in 10 min. Because the fill-time of the sample loops is 6 s, data were not collected at intervals shorter than 10 s. Since most changes in product isotopic composition occur in the first 2 min after the switch in feed isotopic composition, it is desirable to acquire data at intervals shorter than 10 s. To do so, the feed composition was changed from $^{13}CO/D_2$/He to $^{12}CO/D_2$/He and five samples were acquired at 10-s intervals for up to 60 s.

Figure 2 is a schematic of the data acquired during a typical experiment. The curves labeled $F(^{12}C)$ and $F(^{13}C)$ represent the fractions of the carbon atoms that are ^{12}C-labeled and ^{13}C-labeled, respectively. $F(^{12}C)$ is calculated by dividing the ^{12}C concentration observed at a given time by the initial steady-state ^{12}C concentration measured in $^{12}CO/D_2$; $F(^{13}C)$ is obtained by dividing the observed ^{13}C concentration by the ^{13}C concentration measured after 10 min in

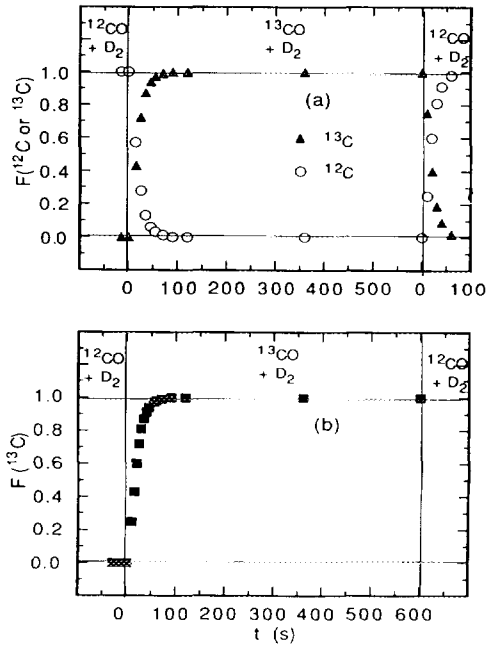

FIG. 2. (a) Data sampling sequence for isotopic transients and (b) composite average rise curve.

$^{13}CO/D_2$. (It had previously been determined that the transients are complete in 10 min.) The sum of $F(^{12}C)$ and $F(^{13}C)$ for a given product always equals 1.0. For the first portion of the experiment, the rise curve points for each product were calculated as the average of the values of $F(^{13}C)$ and $[1\text{-}F(^{12}C)]$, and in the latter section, as the average of the values of $F(^{12}C)$ and $[1\text{-}F(^{13}C)]$. All the points could then be combined to give a rise curve with 16 points. Sampling times were chosen such that data could effectively be collected at 5-s intervals for the first minute after the switch. Data acquired during the initial part of the experiment, as the ^{13}C content in the product rises, was found to be in agreement with data from the latter part of the transient experiment, when the ^{13}C content in the products declines.

THEORETICAL MODELLING

Chain Growth Model

Simulation of the experimentally observed transients was carried out on the ba-

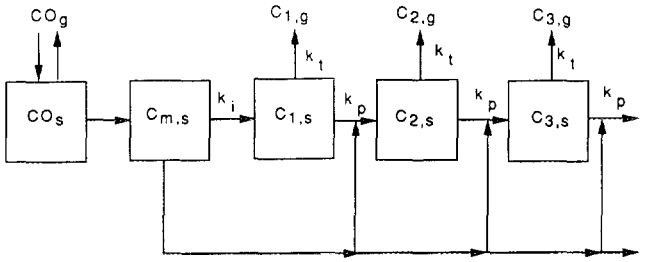

FIG. 3. Chain growth model.

sis of the scheme shown in Fig. 3. This scheme is identical to that used by Zhang and Biloen (*14*) and by Mims and McCandlish (*16*). In Fig. 3, CO_g and CO_s refer to gas-phase and adsorbed CO, $C_{m,s}$ refers to adsorbed monomeric building units, and $C_{n,s}$ and $C_{n,g}$ refer to adsorbed alkyl chains and gaseous products containing n carbon atoms. Reference to reactions 1–16 in the Introduction shows that the scheme in Fig. 3 represents a simplification of the more detailed reaction sequence. First, the species C_s, CH_s, and $CH_{2,s}$ are treated as a common species, C_m, on the assumption that the individual species are in equilibrium with each other. Second, no distinction is made between chain termination to olefins and paraffins. The rate coefficient for conversion of $C_{m,s}$ to $C_{1,s}$ is the apparent first-order rate coefficient for chain initiation, k_i. The rate coefficients k_p and k_t are first-order rate coefficients for chain propagation and termination, respectively. The dependence of any process on adsorbed hydrogen is not shown explicitly, since, for a given set of reaction conditions, the surface coverage of hydrogen is time independent.

Steady-State Rate and Label Balances

The scheme presented in Fig. 3 can be used to derive expressions for F_m and F_n, the fraction of labeled carbon in the monomer pool and in the pool of chains of length n, respectively. Equations for F_m and F_n are obtained in the following manner. A balance on labeled carbon entering and leaving the monomer pool gives

$$\theta_m \frac{dF_m}{dt} = k_d \theta_{CO} F_{CO} - \theta_m F_m (k_i + k_p \sum_{n=1}^{\infty} \theta_n). \quad (1)$$

(In Eq. (1), θ_{CO}, θ_m, and θ_n are the surface coverages for CO, monomeric building units, $C_{m,s}$, and alkyl chains, $C_{n,s}$, respectively.)

At steady state,

$$N_{CO} = k_d \theta_{CO} = k_i \theta_m + k_p \theta_m \sum_{n=1}^{\infty} \theta_n. \quad (2)$$

Combining Eqs. (1) and (2), one obtains

$$\frac{dF_m}{dt} = \frac{F_{CO} - F_m}{\tau_m}, \quad (3)$$

where $\tau_m = 1/(k_i + k_p(\Sigma\theta_n))$.

The appearance and disappearance of labeled carbon in the methane precursor pool C_1 is governed by

$$\theta_1 \frac{dF_1}{dt} = k_i \theta_m F_m - k_t \theta_1 F_1 - k_p \theta_m \theta_1 F_1. \quad (4)$$

Since at steady state

$$k_i \theta_m = k_t \theta_1 + k_p \theta_m \theta_1, \quad (5)$$

Eq. (4) can be rewritten as

$$\frac{dF_1}{dt} = \frac{F_m - F_1}{\tau}, \quad (6)$$

where $\tau = 1/(k_p \theta_m + k_t)$. The appropriate balance on labeled carbon in the pool of alkyl species containing n carbon atoms is given by

$$n\theta_n \frac{dF_n}{dt} = k_p\theta_m\theta_{n-1}[(n-1)F_{n-1} + F_m] - k_p\theta_m\theta_n(nF_n) - k_t\theta_n(nF_n). \quad (7)$$

Once again, at steady state,

$$k_p\theta_m\theta_{n-1} = k_p\theta_m\theta_n + k_t\theta_n, \quad (8)$$

so that Eq. (7) can be rewritten as

$$\frac{dF_n}{dt} = \left(\frac{(n-1)F_{n-1} + F_m}{n} - F_n\right)/\tau. \quad (9)$$

The initial conditions for F_m, F_1, and F_n are $F_m = F_1 = F_n = 0$ at $t = 0$. Since CO is assumed to equilibrate rapidly with the catalyst surface, $F_{CO} = 1$ for $t \geq 0$. With these initial conditions, the solution to Eq. (6) is

$$F_m(t) = 1\text{-}\exp(-t/\tau_m). \quad (10)$$

An analytical solution for $F_n(t)$ can be obtained using Laplace transforms and the convolution theorem (*31*). The resulting expression is

$$F_n(t) = 1.0 + \left(\frac{\exp(-t/\tau_m)}{n}\right) \sum_{i=1}^{n} (-1)^{i-1}\left(\frac{\tau_m}{\tau - \tau_m}\right)^i + \left(\frac{\exp(-t/\tau)}{n}\right) \sum_{i=1}^{n} \frac{1}{\tau^i} \sum_{r=0}^{i-1} \frac{t^{i-r-1}}{(i-r-1)!}\tau^{r+1}\left(\left(-\frac{\tau_m}{\tau-\tau_m}\right)^{r+1} - 1\right). \quad (11)$$

RESULTS AND DISCUSSION

Catalyst Activity and Selectivity

Gas chromatographic analyses of the products taken during the isotopic transient experiments shows that the catalyst activity and selectivity are unchanged over the 11-min duration of the experiment. The main products observed are α-olefins, *cis*- and *trans*-β-olefins, and *n*-paraffins. A few branched products are also detected, but these constitute less than 10% of the total product. Alcohols and other oxygenates are not detected. Mass spectrometric analysis of the products indicates that no CO_2 is formed and that D_2O is the only oxygenated product.

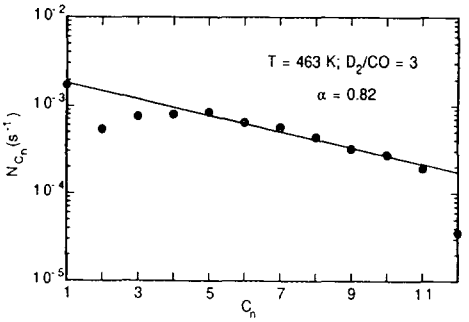

FIG. 4. Anderson–Schulz–Flory plot.

Figure 4 shows an Anderson–Schulz–Flory (ASF) plot of the turnover frequencies for C_1–C_{12} at 463 K and $D_2/CO = 3$. As is characteristic of Ru catalysts (*3, 30*), the points for C_2 and C_3 products fall below the line passing through the points for the C_4–C_{11} products. The point for C_{12} products also lies below the ASF line. This deviation is due to the loss of C_{12} and heavier products in the transfer line to the gas chromatograph, which is maintained at 393 K. A value of $\alpha = 0.82$ is determined from the slope of the line passed through the points for the C_4–C_{11} products.

Figures 5a and 5b show the dependence of the turnover frequency for CO consumption and α on temperature, respectively. N_{CO} is calculated as $\Sigma n N_{C_n}$ for values of n between 1 and 13, and α is taken as the slope of the linear portion of the ASF plot. It is seen from Fig. 5a that N_{CO} exhibits an Arrhenius behavior for temperatures below 473 K and then becomes nearly constant at higher temperatures. Calculations of the Weisz parameter indicate the absence of intraparticle mass-transfer limitations, leading to the conclusion that the observed dependence on temperature is a reflection of the intrinsic kinetics. Figure 5b shows that α decreases monotonically from 0.88 to 0.73 as temperature increases from 453 to 498 K.

The effects of D_2 partial pressure on N_{CO} and α, for a fixed temperature and CO partial

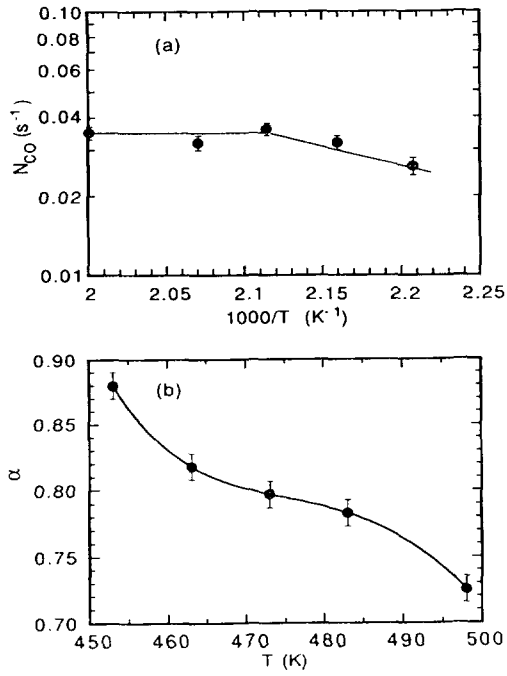

FIG. 5. (a) N_{CO} versus T^{-1} and (b) α vs T: $D_2/CO = 3$.

pressure, are shown in Figs. 6a and 6b. The value of N_{CO} is seen to increase linearly with increasing D_2 partial pressure, whereas the value of α decreases monotonically. The trends reported in Figs. 5b and 6b are similar to those observed previously for Ru/Al_2O_3 (*3*) and for supported Fe catalysts (*4*, *5*).

Figure 7 shows plots of the olefin to paraffin ratios of the C_{2+} hydrocarbons. The olefins to paraffin ratio is essentially independent of temperature, and decreases with increasing D_2/CO ratio.

Isotopic Transients

The incorporation of ^{13}C and the concurrent decline in ^{12}C in the C_1 and C_3–C_8 products was monitored by isotope-ratio GC–MS, following a switch in the feed from $^{12}CO/D_2$ to $^{13}CO/D_2$. The concentration of the C_2 product was too low for mass spectrometric detection. Figures 8 and 9 show representative plots of $F_1(t)$ and $F_n(t)$ (n = 3–8), respectively. The data points in Fig. 9 are based on the measured isotopic fractions in all olefins and paraffins of a given carbon number, since it was observed that the dynamics for products with a given number of carbon atoms could not be differentiated on the basis of structure (i.e., olefin vs paraffin, α-olefin vs β-olefin, n-paraffin vs branched paraffin). Figure 8 shows that the methane transient rises rapidly and approaches 1.0 after 120 s. The transients for C_{3+} shown in Fig. 9 occur on a similar timescale. While there is considerable scatter in the data, it is observed that the appearance of ^{13}C-labeled carbon in the products is progressively slower as the value of n increases from 3 to 8. This trend is particularly evident for the C_{6+} products. The transient for C_8 must be viewed with caution because a part of the C_8 products condense in the transfer line upstream of the capillary combuster. This chromatographic effect introduces an extra delay in the response.

Values of the two parameters τ and τ_m were obtained by fitting the analytical ex-

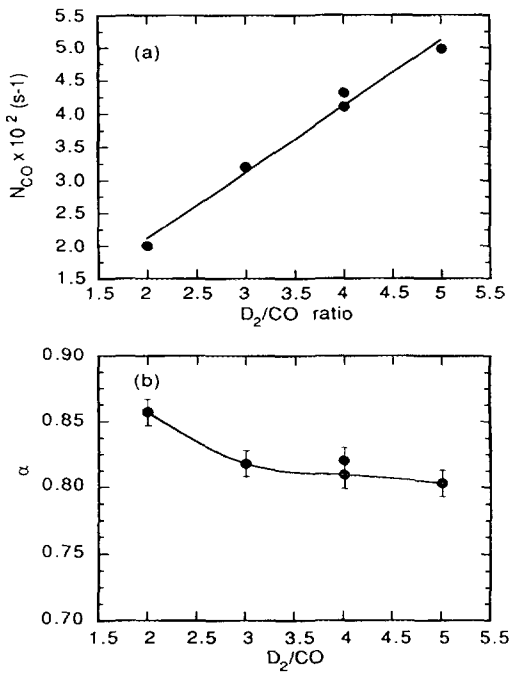

FIG. 6. (a) N_{CO} versus D_2/CO and (b) α vs D_2/CO: T = 463 K.

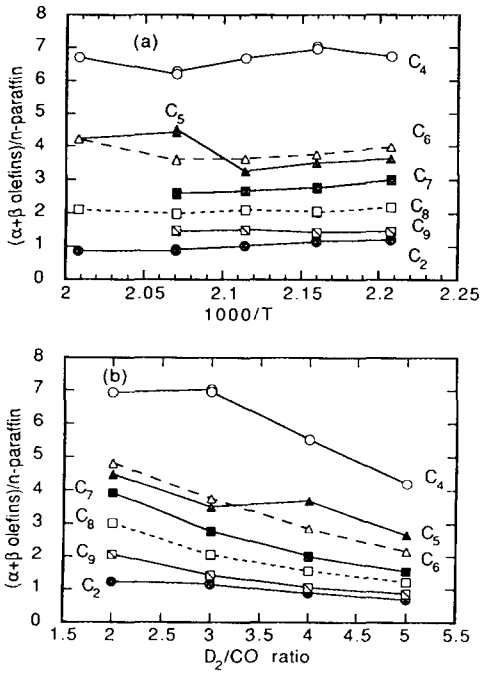

FIG. 7. (a) Ratio of linear olefins to paraffins versus temperature: $D_2/CO = 3$. (b) Ratio of linear olefins to paraffins versus D_2/CO ratio: $T = 463$ K.

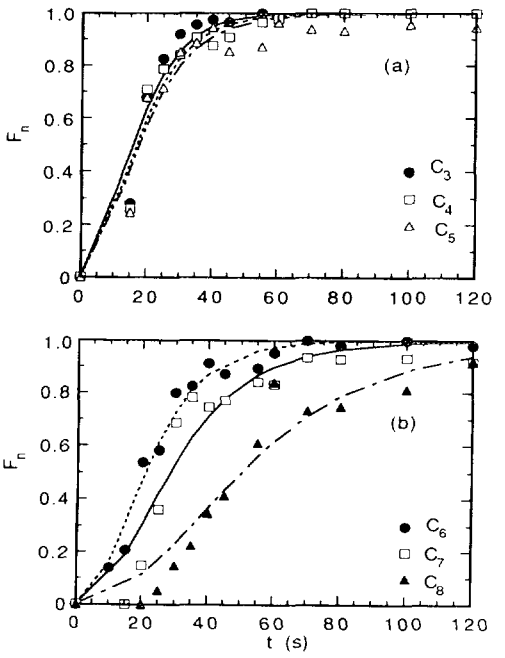

FIG. 9. (a) $F_n(t)$ for $n = 3$–5 and (b) $F_n(t)$ for $n = 6$–8: $T = 463$ K, $D_2/CO = 3$.

pressions for F_n given by Eq. (11) to the experimental data. This was done by using a quasi-Newton method (*31*) to minimize the objective function $S_n(\tau, \tau_m)$ defined as

$$S_n(\tau, \tau_m) = \sum_{j=1}^{M} [F_n^{expt}(t_j) - F_n(t_j)]^2. \quad (12)$$

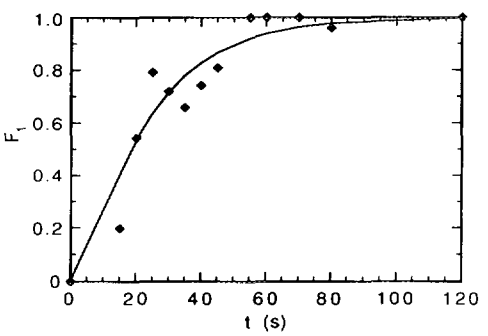

FIG. 8. $F_1(t)$ for CD_4: $T = 463$ K, $D_2/CO = 3$.

In Eq. (12), $F_n^{expt}(t_j)$ and $F_n(t_j)$ are the experimental and theoretical values at time t_j and M is the number of experimental points.

Figures 8 and 9 show data and model fits at a temperature of 463 K and a D_2/CO ratio of 3. The F-test was used to assess the statistical adequacy or lack of fit of the model (*32, 33*). For each value of n, the F-test indicated that the model fit the data at a 95% confidence interval. The parameters τ and τ_m were determined independently for each of the transients from C_1–C_7. Table 1 shows values obtained for the data set at 463 K and $D_2/CO = 3$. It is evident that the values of τ and τ_m determined from different transients exhibit a modest spread in values. The large value of τ_m for $n = 1$ is ascribed to the presence of a 2–3% ^{12}CO impurity in the ^{13}CO feed. This impurity causes an artificial extension of F_1 for long times, as a consequence of the way in which the transient data are acquired (see Fig. 2 and the related text). For these reasons, it was decided that

TABLE 1

Values of τ and τ_m Obtained from Fitting the Chain Growth Model to the Data: $D_2/CO = 3$; $T = 463$ K

Carbon number	τ(s)	τ_m(s)
1	4.7	19.6
3	5.2	7.8
4	3.7	10.3
5	2.8	12.3
6	3.2	12.7
7	3.5	16.7
Average	3.9 ± 0.9[a]	11.9 ± 4.0[b]

[a] Average of values for C_1, C_{3-7}. See text for details.
[b] Average of values for C_{3-7}. See text for details.

average values of τ should be based on the individual values obtained for C_1 and C_{3-7}, and average values of τ_m should be based on individual values obtained for C_{3-7}. It was found that the F_n predictions based on the average values of τ and τ_m were nearly indistinguishable from those based on the best-fit model values for each n from 3–7.

The values of k_i, k_p, and k_t, and θ_m and $\Sigma\theta_n$, can be determined from the values of τ and τ_m, obtained through the fitting procedure described above, and the values of N_{CO}, N_{Cn}, and α obtained from steady-state rate data. The approach used to calculate the rate coefficients and the surface coverages is described in the Appendix.

Figure 10 shows the variation of rate coefficients k_j, k_p, and k_t with T^{-1}. The value of the initiation rate coefficient k_i appears to be independent of temperature. This trend can be rationalized if the initiation of chain growth is assumed to proceed via the process $CH_{2,s} + H_s \rightarrow CH_{3,s}$. In such a case, k_i is an apparent rate coefficient, representing the product of the true rate coefficient, k'_i, and the coverage of adsorbed hydrogen, θ_H. Since k'_i is expected to increase with increasing temperature but θ_H is expected to decrease, the product of k'_i and θ_H should be less sensitive to temperature than either of the two factors making up the product. The plots of k_p and k_t vs T^{-1} both have negative slopes, from which it is determined that the activation energy for chain propagation, E_p, is 8 kcal/mol and the activation energy for chain termination E_t, is 20 kcal/mol.

The present evaluation of k_p can be compared to the estimated apparent rate of propagation reported by Zhang and Biloen (*14*). To do so, k_p is multiplied by θ_m (see below) to obtain $k_p^{app} = k_p\theta_m$. For the data presented in Fig. 10, k_p^{app} lies between 0.25 and 0.5 s^{-1}. This range lies somewhat below Zhang and Biloen's estimate of >1 s^{-1}. There is close agreement between the values of k_t reported here and in the work of Yokomizo and Bell (*21*). Using an Ru/TiO_2 catalyst similar to that described here, Yokomizo and Bell determined a value of $k_t = 0.044 s^{-1}$ at $T = 463$ K, from modelling of temperature programmed surface reaction (TPSR) data. For the same reaction conditions, we obtain a value of $k_t = 0.047$ s^{-1}.

The activation energy for chain termination (20 kcal/mol) is significantly higher than that for chain propagation (8 kcal/mol). This explains why the value of α decreases with increasing temperature (see Fig. 5b). While

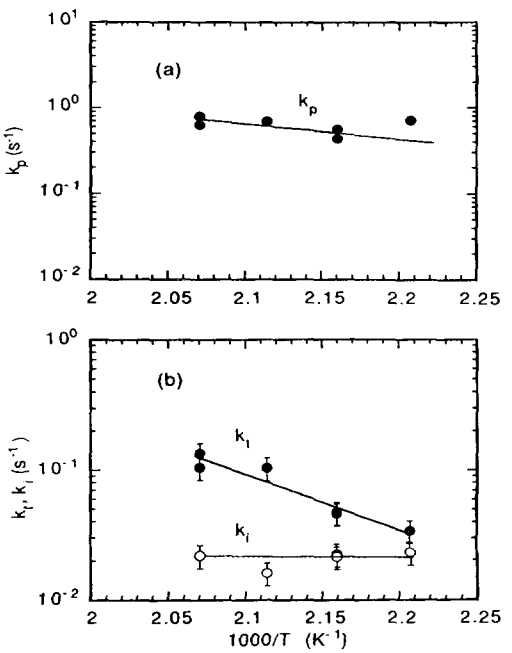

FIG. 10. (a) k_p and (b) k_i and k_t vs T^{-1}: $D_2/CO = 3$.

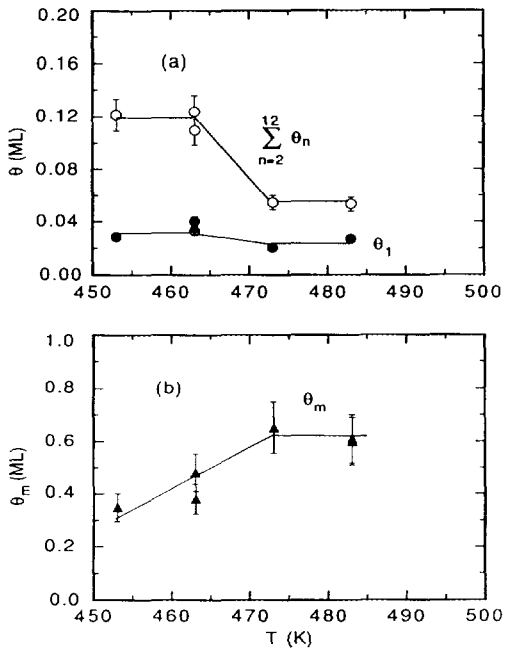

FIG. 11. (a) $\Sigma n\theta_n$ and (b) θ_m vs T: $D_2/CO = 3$.

experimental values of E_t and E_p have not been reported in the literature previously, Shustorovich and Bell (*34*) have shown using the Bond-Order-Conservation-Morse-Potential (BOC-MP) approach, that E_t should be larger than E_p for Ni and Fe. Thus, for Ni(111), E_p for the chain growth step to form a C_2 species is estimated to be 6 kcal/mol, whereas E_t is estimated to be 11 kcal/mol for chain termination to ethylene and 19 kcal/mol for chain termination to ethane. For Fe(110), E_p for the formation of C_2 species is estimated to be 20 kcal/mol, whereas E_t is estimated to be 16 kcal/mol for chain termination to ethylene and 32 kcal/mol for chain termination to ethane.

The effects of temperature on the calculated values of surface coverage by carbonaceous species is given in Fig. 11 and Table 2. The values of θ_m lie between 0.3 and 0.6 ML, while the value of $\Sigma\theta_n$ lies between 0.12 and 0.05 ML. It is observed that with increasing temperature, θ_m increases, but θ_1 and $\Sigma\theta_n$ decrease. These trends are consistent with the observed temperature dependences for chain initiation, propagation, and termination. As seen in Fig. 10, increasing temperature has virtually no effect on k_i, but increases both k_p and k_t. Since E_t is larger than E_p, the rate of chain termination increases more rapidly than the rate of chain propagation, with the result that the surface coverage by growing alkyl chains decreases, whereas the coverage by monomeric building units increases. The total coverage by reaction intermediates is seen to be between 0.5 and 0.7 of a monolayer.

To determine whether or not the surface coverages estimated from the model are representative of actual coverages by carbonaceous species, a series of temperature-programmed surface reactions were carried out. Using the techniques described in Ref. (*27*), measurements were made of the CO uptake capacity of the freshly reduced catalyst, the CO uptake of the catalyst after 20 min under reaction conditions, and the total carbon inventory on the catalyst surface, exclusive of CO, after 20 min under reaction conditions. The room-temperature uptake of CO on the freshly reduced catalyst is 1.3 ML. After 20 min of reaction at 463 K and a D_2/CO ratio of 3, the CO coverage decreases to 0.67 ML and the total amount of carbon exclusive of CO is 1.08 ML. The last of these figures compares very favorably with the value of $\Sigma n\theta_n = 1.03$ obtained from the simulation of the transient response experiments. Moreover, the sum of θ_{CO} plus $\Sigma\theta_n$ for $n = 1$–13 is equal to 1.19–1.31 ML (see Table 2), in good agreement with the initial CO uptake capacity of the catalyst, 1.3 ML. A similar level of agreement is observed when the reaction is carried out at 483 K.

The close correspondence between the predicted and experimentally observed coverages by carbon indicates that the dynamics of the transient response experiments are governed primarily by the α (carbidic) and β' (growing alkyl chains) forms of surface carbon (*21*). As noted by Krishna and Bell (*27*), these forms of carbon exhibit time

TABLE 2

The Effect of Temperature on the Coverage by Reaction Intermediates: $D_2/CO = 3$

T(K)	θ_1(ML)	$\sum_{n=2}^{12} \theta_n$(ML)	θ_m(ML)	Total $\theta_{(n+m)}$(ML)	θ_{CO}(ML)
453	0.03	0.12	0.35	0.5	—
463	0.03	0.11	0.38	0.52	0.67
463	0.04	0.12	0.48	0.64	0.67
473	0.02	0.05	0.62	0.69	—
483	0.03	0.05	0.61	0.69	0.65
483	0.03	0.61	0.60	0.68	0.65

constants that are much shorter than that associated with the build up and consumption of β'' carbon, which contributes to the slow deactivation of Ru.

The observation of a higher surface coverage by monomeric units than by growing chains is qualitatively consistent with the findings of Yokomizo and Bell (*21*) for Ru/TiO_2 and Mims and McCandlish (*16*) for Co/Al_2O_3. Yokomizo and Bell (*21*) estimate the surface coverage by all C_1 species to be 0.25 ML and the coverage by C_{2+} chains to be about 0.10 ML. This compares favorably with the present results which indicate a surface coverage of 0.12 ML by C_{2+} species and a coverage of 0.4 by all C_1 species. Since the estimates of surface coverages reported here and by Yokomizo and Bell (*21*) are based on completely different methods, the degree of agreement is all the more remarkable.

Figure 12 indicates the effects of D_2 partial pressure on k_1, k_p, and k_t. The value of k_p is essentially independent of the partial pressure of D_2, consistent with what would be expected, since chain growth does not involve adsorbed D atoms. By contrast, the value of k_t rises linearly with increasing D_2 partial pressure. This trend can be explained in the following manner. As defined k_t is an apparent rate coefficient representing termination to olefinic and paraffinic products. Expressing k_t in terms of its component parts gives

$$k_t = k_t^{=}\theta_v + k_t^{-}\theta_D, \qquad (13)$$

where $k_t^{=}$ and k_t^{-} are the rate coefficients for termination to olefins and paraffins, respectively, and θ_v and θ_D are the vacancy and D atoms surface coverages, respectively. The increase in k_t with D_2 partial pressure can, therefore, be attributed to the increase in θ_D. In agreement with this, the product distribution shifts to more paraffinic products as the D_2 partial pressure rises (see Fig. 7). Equation (13) also helps explain the weak dependence of the olefin to paraffin ratio

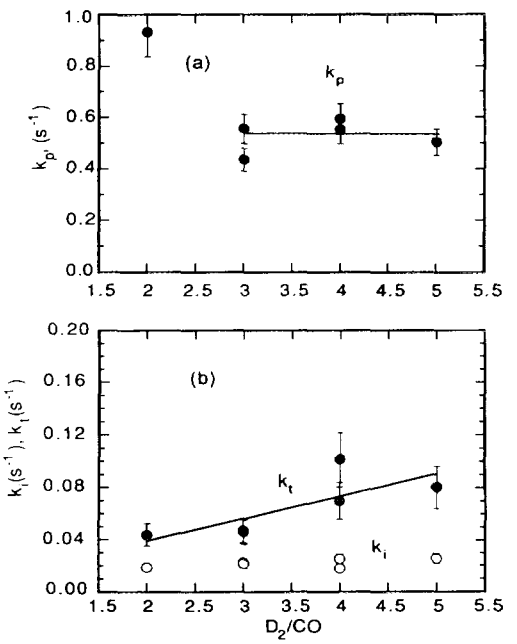

FIG. 12. (a) k_p and (b) k_t vs D_2/CO: $T = 463$ K.

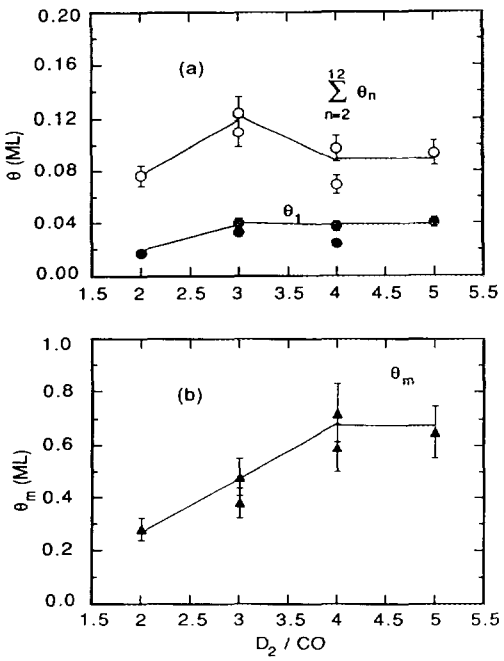

FIG. 13. (a) $\Sigma n\theta_n$ and (b) θ_m vs D_2/CO: T = 463 K.

on temperature, seen in Fig. 7. Since θ_D decreases and k_t^- increases with temperature, the product of θ_D and k_t^- should show a weaker temperature dependence.

The independence of k_i on D_2 partial pressure is puzzling, since as discussed above, this rate coefficient is, in fact, the product of an intrinsic rate coefficient and θ_D. No explanation can be given for why k_i does not behave in the same manner as k_t.

The dependence of the surface coverages of carbonaceous species calculated from the model is given in Fig. 13 and Table 3. The coverage by monomeric building units and C_1 chain initiators increases with D_2 partial pressure and approaches a constant value, whereas the surface coverage by C_{2-12} chains appears to pass through a maximum. The trends in θ_m and θ_1 indicate that with decreasing D_2 partial pressure, the rate of conversion of nascent carbon atoms to CH_x species is somewhat faster than the consumption of these species to form reaction products. The total coverage by reactive species is seen to increase from 0.4 to 0.8 ML as the D_2/CO ratio changes.

CONCLUSIONS

Isotopic tracer methods have been used to determine the dynamics of chain initiation, propagation and termination for Fischer–Tropsch synthesis over Ru/TiO_2. Values for the rate coefficients k_i, k_p, and k_t were determined by fitting theoretically generated transient response curves to those obtained experimentally. The rate coefficient for chain initiation, k_i, is independent of both temperature and D_2/CO ratio. The rate coefficient for chain propagation, k_p, has an activation energy of 8 kcal/mol, but is independent of the D_2/CO ratio. The rate coefficient for chain termination, k_t, has an activation energy of 20 kcal/mol and increases linearly with D_2/CO ratio. The higher activation energy for chain termination than that for chain propagation explains the observed decrease in probability of chain growth, α, with increasing temperature.

The surface coverages by various carbonaceous species have also been determined from an analysis of the fitted transient response curves. It is concluded that the dominant species are monomeric building units, which occupy 0.2 to 0.6 ML. Growing alkyl chains, the direct precursors to hydrocarbon products occupy $\leq$ 0.2 ML. Adsorbed CO occupies an additional $\approx$0.7 ML. These estimates are found to be in good agreement with independent measurements made by temperature-programmed reaction spectroscopy.

APPENDIX

The apparent rate constant for propagation, $k_p\theta_m$, and the rate constant for termination, k_t, are calculated from α and τ using the following equations:

$$\alpha = \frac{k_p \theta_m}{k_p \theta_m + k_t} \qquad \text{(A1)}$$

and

TABLE 3

The Effect of D_2/CO Ratio on the Coverage by Reaction Intermediate: T = 463 K

D_2/CO	θ_1(ML)	$\sum_{n=2}^{12} \theta_n$(ML)	θ_m(ML)	Total $\theta_{(n+m)}$(ML)
2	0.03	0.12	0.28	0.43
3	0.03	0.11	0.38	0.52
3	0.04	0.12	0.48	0.64
4	0.02	0.07	0.72	0.81
4	0.04	0.10	0.59	0.73
5	0.04	0.10	0.65	0.79

$$\tau = \frac{1}{k_p \theta_m + k_t}. \tag{A2}$$

The value of τ is determined from a fit of Eq. (12) to the observed curves of $F_n(t)$.

The monomer coverage, θ_m, is calculated as follows. At steady state, the rate of CO consumption must equal the rate at which monomeric species are consumed. This equality can be written as

$$N_{CO} = \frac{\theta_m}{\tau_m}. \tag{A3}$$

Since N_{CO} is known from steady-state rate measurements and τ_m is known from the fit of Eq. (12) to the observed curves $F_n(t)$, θ_m can be evaluated. The value of k_p can be determined from Eq. (A2).

The value of k_i can be calculated by recognizing that the rate at which carbon atoms are consumed from the C_1 pool is equal to the rate at which carbon atoms enter this pool. This leads to Eq. (A4),

$$\frac{\theta_1}{\tau} = k_i \theta_m. \tag{A4}$$

Since

$$\frac{\theta_1}{\tau} = \frac{N_{C_1}}{k_t} \Big/ \frac{1}{k_p \theta_m + k_t} = \frac{N_{C_1}}{1 - \alpha}, \tag{A5}$$

k_i can be calculated from Eqs. (A4) and (A5), using the measured values of N_{C_1} and α, and the previously determined value of θ_m.

The coverages by alkyl species can be calculated from the hydrocarbon turnover frequencies and the value of k_t. Since

$$N_{Cn} = k_t \theta_n, \tag{A6}$$

then

$$\sum_{n=1}^{n_1} \theta_n = \frac{1}{k_t} \sum_{n=1}^{n_1} N_{C_n} \tag{A7}$$

ACKNOWLEDGMENTS

The authors thank R. L. June for the computer program used to minimize the objective function and to obtain modelling parameters. This work was supported by the Director, Office of Basic Energy Sciences, Chemical Sciences Division of the U.S. Department of Energy under Contract DE-AC03-76SF00098.

REFERENCES

1. Anderson, R. B., "The Fischer–Tropsch Synthesis." Academic Press, New York, 1984.
2. Biloen, P., and Sachtler, W. M. H., *Adv. Catal.* **30,** 165 (1981).
3. Kellner, C. S., and Bell, A. T., *J. Catal.* **70,** 418 (1981).
4. Dry, M. E., *Catal. Sci. Technol.* **1,** 150 (1981).
5. Dry, M. E., *Catal. Today* **6,** 183 (1990).
6. Bell, A. T., *Catal. Rev.-Sci. Eng.* **23,** 203 (1981).
7. Winslow, P., and Bell, A. T., *J. Catal.* **86,** 158 (1984).
8. Winslow, P., and Bell, A. T., *J. Catal.* **91,** 142 (1985).
9. Biloen, P., Helle, J. N., and Sachtler, W. M. H., *J. Catal.* **58,** 95 (1979).
10. Bonzel, H. P., and Krebs, H. J., *Surf. Sci.* **91,** 499 (1980).
11. Kobori, Y., Yamasaki, H., Naito, S., Onishi, T., and Tamaru, K., *J. Chem. Soc., Faraday Trans. I* **78,** 1473 (1982).

12. Biloen, P., Helle, J. N., van den Berg, F. G. A., and Sachtler, W. M. H., *J. Catal.* **81,** 450 (1983).
13. Orita, H., Naito, S., and Tamaru, K., *J. Catal.* **90,** 183 (1984).
14. Zhang, X., and Biloen, P., *J. Catal.* **98,** 468 (1986).
15. Mims, C. A., and McCandlish, L. E., *J. Am. Chem. Soc* **107,** 696 (1985).
16. Mims, C. A., and McCandlish, L. E., *J. Phys. Chem.* **91,** 929 (1987).
17. Stockwell, D. M., and Bennett, C. O., *J. Catal.* **110,** 354 (1988).
18. Stockwell, D. M., Bianchi, D., and Bennett, C. O., *J. Catal.* **113,** 13 (1988).
19. Biloen, P., *J. Mol. Catal.* **21,** 17 (1983).
20. Bennett, C. O., *in* "Catalysis under Transient Conditions" (A. T. Bell and L. L. Hegedus, Eds.), ACS Symposium Series, Vol. 178, p. 1. ACS, Washington, DC, 1982.
21. Yokomizo, G. H., and Bell, A. T., *J. Catal.* **119,** 467 (1989).
22. Vannice, M. A., *J. Catal.* **37,** 449 (1975).
23. Vannice, M. A., and Garten, R. L., *J. Catal.* **56,** 236 (1979).
24. Vannice, M. A., and Sudhakar, C., *J. Phys. Chem.* **88,** 2429 (1984).
25. Reuel, R. C., and Bartholomew, C. H., *J. Catal.* **85,** 78 (1984).
26. Rieck, J. S., and Bell, A. T., *J. Catal.* **99,** 262 (1986).
27. Krishna, K. R., and Bell, A. T., *J. Catal.* **130,** 597 (1991).
28. Sano, M., Yotsui, Y., Abe, H., and Sasaki, S., *J. Biomed. Mass Spectrosc.* **3,** 1 (1976).
29. Matthews, D. E., and Hayes, J. M., *Anal. Chem.* **50,** 1465 (1978).
30. Jordan, D. S., and Bell, A. T., *J. Phys. Chem.* **90,** 4797 (1986).
31. Jenson, V. G., and Jeffreys, G. V., "Mathematical Methods in Chemical Engineering," 2nd ed. Academic Press, 1977.
32. Froment, G. F., and Hosten, L. H., *Catal. Sci. Technol.* **2,** 97 (1981).
33. Box, G. E. P., Hunter, W. G., and Hunter, J. S., "Statistics for Experimenters." Wiley, New York, 1978.
34. Shustorovich, E., and Bell, A. T., *Surf. Sci.* **248,** 359 (1991).